Carbohydrate Polymers 369 (2025) 124292

Contents lists available at ScienceDirect

Carbohydrate Polymers

journal homepage: www.elsevier.com/locate/carbpol

Characterizing maize starch gelatinization by Low-Field NMR spectroscopy

Li Ding [a], Samira Ebrahimi [a,c], Xingxun Liu [d], Staffan Persson [a,e], Jacob Judas Kain Kirkensgaard [b,c], Kasper Enemark-Rasmusse [f], Jinhui Chang [g], Sheng Chen [g], Andreas Blennow [a], Tomasz Pawel Czaja [b,*], Yuyue Zhong [a,g,**]

[a] Copenhagen Plant Science Center, Department of Plant and Environmental Sciences, Faculty of Science, University of Copenhagen, Denmark
[b] Department of Food Science, University of Copenhagen, DK-1958 Frederiksberg C, Denmark
[c] Niels Bohr Institute, University of Copenhagen, DK-2100 Copenhagen Ø, Denmark
[d] Lab of Food Soft Matter Structure and Advanced Manufacturing, College of Food Science and Engineering, Nanjing University of Finance and Economics, Nanjing 210023, China
[e] Joint International Research Laboratory of Metabolic & Developmental Sciences, State Key Laboratory of Hybrid Rice, SJTU-University of Adelaide Joint Centre for Agriculture and Health, School of Life Sciences and Biotechnology, Shanghai Jiao Tong University, Shanghai, China
[f] Department of Chemistry, Technical University of Denmark, DK-2800, Kemitorvet, Building 207, Kgs. Lyngby, Denmark
[g] Department of Food Science and Nutrition, The Hong Kong Polytechnic University, Hung Hom, Kowloon, Hong Kong, China

ARTICLE INFO

Keywords:
LF-NMR
gelatinization
water mobility
amylose content
starch-water interactions

ABSTRACT

Transverse relaxation time (T_2) of starch, measured by low-field nuclear magnetic resonance spectroscopy (LF-NMR), were analyzed to understand starch swelling and gelatinization. Three water proton populations were identified: T_{21} (intra-granular water), T_{22} (extra-granular water on the granular surface), and T_{23} (free water or leached-starch interacting water). During heating at 40 °C or 60 °C, where granular swelling occurred, the relative proton concentration of T_{22} (M_{22}) and T_{21} decreased, while M_{21} increased. At 80 °C, where gelatinization happened, M_{21} and T_{21} increased and then decreased to stable values, opposite to the trend of M_{22}. These observations suggest that starch swelling is facilitated by the migration of extra-granular water into intra-granular regions, while gelatinization is driven by the redistribution of intra-granular water back to extra-granular regions. Across all temperatures, T_{23} and M_{23} increased and then remained stable. Higher AC retarded and prolonged both processes, by restricting T_{21} while enhancing T_{22}. Pearson correlation analysis further suggested that M_{21} was positively correlated with relative content of amorphous region in raw starches, while after heating, M_{21} had positive correlations with 1047/1022 ratio of the FTIR absorbances and gelatinization temperatures. These findings offer insights into applying LF- NMR in evaluating starch gelatinization dynamics.

1. Introduction

Starch, composed of two macromolecules, linear amylose (AM) and highly branched amylopectin (AP), is a primary storage carbohydrate in plants and is widely used in the food industry as a stabilizer, thickener, and texturizer (Luallen, 2018). Gelatinization, one of the most critical properties of starch, regulates the functionality of all starch-based foods cooked in excess water. Gelatinization is a process induced by water and heat, during which starch transitions from a semi-crystalline to an amorphous and solubilized state. This transformation is characterized by water absorption, swelling of AP, melting and hydration of crystallites, leaching of starch molecules, and the eventual collapse of the granule structure (Zhang et al., 2014). Hence, gelatinization properties of starch are vital for the quality, acceptability, nutritional value, and shelf-life of starch-based foods, making a clear understanding of this process essential for starch food processing.

Various techniques have been employed to characterize starch gelatinization, including differential scanning calorimetry (DSC) (Wang, Zhang, Wang, & Copeland, 2016), Rapid Visco-Analysis (RVA) (Guo et al., 2024), rheometry (Sikora et al., 2010), nuclear magnetic resonance (NMR), optical and polarized microscopy (Ding et al., 2019), small-angle X-ray scattering (SAXS) (Xu et al., 2021), and X-ray

* Corresponding author.
** Correspondence to: Y. Zhong, Copenhagen Plant Science Center, Department of Plant and Environmental Sciences, Faculty of Science, University of Copenhagen, Denmark.
E-mail addresses: tomasz.czaja@food.ku.dk (T.P. Czaja), yuyuezhong93@163.com (Y. Zhong).

https://doi.org/10.1016/j.carbpol.2025.124292
Received 2 May 2025; Received in revised form 19 July 2025; Accepted 25 August 2025
Available online 26 August 2025

diffractometry (XRD) (Ai & Jane, 2015). Each technique offers distinct advantages and limitations. For instance, solid-state NMR, polarized microscopy, SAXS, and XRD are primarily used to assess changes in starch structural orders, RVA and rheometry focus on granular and molecular interactions, while DSC is particularly useful for analyzing crystal melting during the process (Li, 2022; Wang & Copeland, 2013). However, these methods are limited in their ability to capture how water, a critical factor in gelatinization, interacts with starch. Low-field nuclear magnetic resonance (LF-NMR) is one promising technique that could address this gap, though it has not been widely applied in starch gelatinization studies.

LF-NMR, as a noninvasive and nondestructive technique, is a widely analytical tool to analyze the interaction of protons with electromagnetic radiation in the radio frequency range, providing various signals, such as longitudinal relaxation time (T_1) or transverse relaxation time (T_2) (Kirtil, Cikrikci, McCarthy, & Oztop, 2017). To some content, LF-NMR has been used to monitor water mobility and distributions of starch in foods, such as bread (Bosmans et al., 2012; Nivelle, Beghin, Bosmans, & Delcour, 2019), dough (Doona & Baik, 2007; Rondeau-Mouro et al., 2014) and biscuit (Serial et al., 2016), although Bosmans et al. (2012) also includes relevant findings on pure starch. However, the complex distribution of components in these foods, along with potential interactions and competitions between starch molecules and other macromolecules, such as lipids and proteins, makes understanding starch-water interactions challenging. Thus, the use of pure starches will provide a direct means of examining starch-water interactions.

Among the parameters obtained from LF-NMR measurements, T_2 relaxation time reflects the time it takes for the transverse magnetization to decay to 37 % of its initial value, primarily due to dephasing of nuclear spins caused by dipole-dipole interactions, providing insight into molecular mobility and interactions (Wu et al., 2018). T_2 relaxation time has been shown to be a key indicator related to starch swelling and gelatinization during heating. During gelatinization, processes such as water uptake and granular swelling, driven by starch-water interactions, can be effectively monitored through changes in T_2 time constants. For example, previous studies have shown that shifts between proton populations and decreased proton mobility at lower heating temperatures (20–50 °C) are associated with starch swelling and AM leaching, while at higher temperatures (60–90 °C), these changes are primarily attributed to starch gelatinization and the disruption of starch granules (Kovrlija, Goubin, & Rondeau-Mouro, 2020; Nivelle, Beghin, et al., 2019). However, most previous studies using LF-NMR on starch have focused on tracking T_2 changes as heating temperatures increase (Kovrlija et al., 2020; Rondeau-Mouro et al., 2014; Serial et al., 2016). While the specific relationships between T_2 time constants and starch structural changes during swelling and gelatinization remains to be investigated, limiting the broader utility of LF-NMR in understanding this process. In addition, AM is a negative regulator for water absorption, starch swelling and gelatinization, but positive regulator for maintaining intact granular structures during heating (Nivelle et al., 2019; Zhong et al., 2022; Zhu et al., 2016). Previous research has shown that different starch types, characterized by varying AM content (AC), produce distinct LF-NMR proton relaxation during gel formation and retrogradation (Thygesen, Blennow, & Engelsen, 2003). Therefore, we hypothesized that T_2 relaxation times, influenced by AC, are correlated with starch gelatinization properties.

In the current study, T_2 relaxation profiles of waxy, normal, and high-amylose maize starches in excess water were measured using LF-NMR at various temperatures ranging from 40 to 80 °C. The possible relevant properties (thermal properties, swelling power and water solubility) and structures (molecular, helical, crystalline and lamellar structures) of starches were also measured for further interpreting the T_2 relaxation time constants during starch gelatinization. Our findings highlight the potential of further employing LF-NMR to understand starch gelatinization via revealing starch-water interactions.

2. Materials and methods

2.1. Materials

Three maize starches with varied AC were selected, including waxy (WMS), normal (NMS), and high AM (HAMS) maize starches. NMS (Commercial Clinton 106) was kindly provided by Archer Daniels Midland (ADM, Decatur, IL), while WMS and HAMS (Hylon VII) were provided by the College of Agronomy at Northwest A&F University, Yangling, Shaanxi, China. The apparent AC determined by the iodine complexation method of WMS, NMS, and HAMS were 0.7 %, 27.4 %, and 69.3 %, respectively (Table S1). Isoamylase (EC 3.2.1.68, *E*-ISAMY, 200 units / mL) was purchased from Megazyme (K-TSTA, Megazyme, Co. Wicklow, Ireland). All other chemicals used in this study were of analytical grade.

2.2. LF-NMR measurements of starches heated in excess water at different temperatures

LF-NMR relaxation curves of starch samples heated in excess water at 40 °C, 60 °C and 80 °C was determined using a MQR Spectro-P LF-NMR spectrometer (Oxford Instruments, Oxfordshire, UK) with an operating frequency of 20.5 MHz (0.47 T). To minimize temperature fluctuations during NMR measurement, 4.5 g of water in an NMR tube was preheated to the desired temperature (40–80 °C) before adding the 0.5 g of starch powder. After equilibration for 1 min, the starch solution was placed in the NMR instrument. All NMR tubes were tightly sealed with Parafilm during the entire course of the experiments to minimize water evaporation. All samples were evaluated with Carr-Purcell-Meiboom-Gill (CPMG) pulse sequence. The relaxation curves were recorded every two minutes during the 1 h of heating to obtain kinetic curves. The pulse parameters were set as follows: recycle delay 8 s, τ- delay 800 μs, 8000 echoes, and 8 scans. After 1 h of measurements, starch samples were immediately snap freezing in liquid nitrogen, freeze-dried, and gently ground for further multi-structural analyses, denoted as 1 h-heated starch samples.

Exponential fitting of the relaxation curves was applied by an in-house MATLAB (2022a, MathWorks, MA, USA) script based on the following equation:

$$I(t) = \sum_{i=1}^{N} M_{2n} {}^{*} e^{-t/T_{2n}}$$

Where I(t) corresponds to the echo intensity with increasing time, N is the number of proton populations in the sample determined by visual inspection of residuals following model fitting, T_{2n} is the transverse relaxation time of component n, and M_{2n} is the corresponding relative proton concentration (Vickovic et al., 2023). Analyses were performed in duplicates, where each spectrum was fitted individually, and the averaged values of the spectra were plotted. Three proton populations were observed in starch samples, including T_{21}, T_{22} and T_{23}, and their relative proton concentrations were denoted as M_{21}, M_{22}, and M_{23}, respectively.

2.3. Chain length distribution (CLD)

A high-performance anion exchange chromatography-pulsed amperometric detection system (HPAEC-PED, Dionex, Sunnyvale, CA, USA) was employed to analyze the distribution of chain length. Briefly, 5 mg of starch was suspended in 1 mL of 100 mM acetate buffer (pH 4.0). The full gelatinization of starch samples was achieved by heating at 99 °C for WMS and NWS sample or at 130 °C for HAMS sample for 1 h with manually shaking every 10 mins. The obtained starch paste was debranched through a three-hour-incubation at 40 °C with 0.4 U isoamylase under the 500 rpm of shaking, and another ten-minute-incubation at 99 °C was done to deactivate the enzyme. Finally, 40 μL

of the debranched supernatant was injected into a CarboPac PA-200 column at a flow rate of 0.4 mL per minute. The program for running the samples was as described in (Tian et al., 2024). The obtained CLD of AP was divided into four fractions: fa (DP 6–12), fb1 (DP 13–24), fb2 (DP 25–36), and fb3 (DP > 36) chains.

2.4. Thermal properties

The thermal properties of raw and 1 h-heated starch samples were measured by a differential scanning calorimeter (DSC1, Mettler Toledo, Schwerzenbach, Switzerland). Starch (5 mg) were weighed into standard aluminum (WMS and NMS samples) or medium-pressure stainless-steel crucibles (HAMS samples), and then 15 μL of MilliQ water was added, followed by seal and equilibration at 4 °C overnight. The pans were heated from 30 to 120 °C (WMS and NMS samples) or to 180 °C (HAMS samples) with a heating rate of 10 °C per minute using an empty pan as reference.

2.5. Swelling power (SP) and water solubility (WS)

20 mg of raw and 1 h-heated starch samples were incubated at 50 °C for 1 h with 0.5 mL MilliQ water. After cooling to ambient temperature, the starch samples were subjected to a centrifugation at 20,000 *g* for 20 min to obtain the swollen starches, and the supernatant was carefully collected and dried at 120 °C overnight. The swollen starches and dried supernatant were weighed and denoted as m1 and m2, respectively. SP and WS were calculated using the eq. 1 and 2, respectively.

$$SP(g/g) = \frac{m1 - 20}{20} \tag{1}$$

$$WS(\%) = \frac{m2}{20} \tag{2}$$

2.6. Helical structures

The helical structures of raw and 1 h-heated starch samples were determined using a solid-state ^{13}C NMR spectrometer (Bruker AV-600, Faellanden, Switzerland). Spectra were measured at 14.1 T Bruker AVIIIHD spectrometer at a ^{13}C frequency of 150.9 MHz with the same parameter settings as described previously (Ding et al., 2023). Amorphous reference was prepared by fully gelatinization of WMS suspensions (1 % *w/v*) in MilliQ water for 1 h at 99 °C, followed by snap freezing in liquid nitrogen and lyophilization. The raw NMR spectra were decomposed into respective amorphous and ordered sub-spectra by subtracting the spectra of amorphous references at about 85 ppm, and the relative amounts of single helices (102–103 ppm), double helices (99–101 ppm), and amorphous regions were calculated separately.

2.7. Crystalline and lamellar structures

The raw and 1 h-heated starch samples were equilibrated at 90 % relative humidity for one week, and their crystalline structures were analyzed by a wide-angle X-ray scattering (WAXS) instrument (Nano-inXider, Xenocs SAS, Grenoble, France) equipped with a Cu Kα source with a 1.54 Å wavelength and a two-detector setup. The total relative crystallinities were calculated using PeakFit 4.0 (Systat Software Inc., San Jose, CA, USA) as described in (Ding et al., 2023).

Small-angle X-ray scattering (SAXS) analysis was conducted to obtain the lamellar structures, including the thickness of the crystalline (d_c), amorphous (d_a) lamellae, long period distance (d_{ac}), and Bragg lamellar repeat distance (D), using the same instrument as above, and following the protocol of (Kuang et al., 2017; Tian et al., 2024).

2.8. Short-range order structures

A MB100 Fourier Transform Infrared (FTIR) spectrometer (ABB-Bomem, Quebec, Canada) equipped with an attenuated total reflectance (ATR) single reflectance cell with a diamond crystal was used to analyze starch short-range order bonding structure. Sixty-four scans were applied for each starch sample from 4000 to 500 cm^{-1} at a resolution of 8 cm^{-1} with background air. The deconvolution of each FTIR spectrum spanning from 1200 to 800 cm^{-1} was achieved using OMNIC 8.0 (Thermo Fisher Scientific Inc., Madison, WI) with a half-bandwidth of 19 cm^{-1} and an enhancement factor of 1.9. The short-range order, as represented by ratio of absorbance at 1047 cm^{-1} to 1022 cm^{-1}, was calculated using the eq. 3.

$$Short\_range\ order = \frac{\text{Absorbance at } 1047\ cm^{-1}}{\text{Absorbance at } 1022\ cm^{-1}} \tag{3}$$

2.9. Morphological structures

Light images were performed using an inverted light microscope (Nikon, Eclipse Ti2) under both bright-field illumination and dark-field differential interference contrast (DIC) mode where the polarizer and analyzer have been adjusted at cross-polarization state. A 40× microscope objective lens (Plan Apo, $NA = 0.95$) was used for magnification and the images were captured by a sCMOS camera (Hamamatsu, ORCA Flash 4.0, 2048 × 2048 pixel array and 6.5 μm pixel-pitch).

2.10. Statistical analysis

The experiments were performed at least in duplicates, and the results were presented as means ± standard deviations. Pearson's correlations and analysis of Variance (ANOVA) with Duncan's test were conducted using SPSS 25.0 software (SPSS, Inc. Chicago, IL, USA). Flow diagram of the experimental design in this study is shown in Fig. 1.

3. Results and Discussion

To select suitable temperatures for observing changes in starch swelling and gelatinization, thermal properties of three raw starches were measured by DSC and are presented in Table 1. The gelatinization temperatures of WMS and NMS ranged from 64.8 °C to 77.4 °C and 64.8 °C to 73.9 °C, respectively. Therefore, three heating temperatures were selected: 40 °C (below the gelatinization temperature), 60 °C (sub-gelatinization temperature), and 80 °C (above the gelatinization temperature) to acquire **LF-NMR** relaxation curves and monitor structural changes related to starch swelling and gelatinization. However, HAMS exhibited significantly higher gelatinization temperatures, ranging from 82.4 °C to 110.7 °C, which exceeded the heating range (20 °C to 90 °C) of the LF-NMR system. Thus, its gelatinization process could not be fully captured.

3.1. Multi-scale structural changes of 1 h-heated starch samples

To understand the water absorption, starch swelling and gelatinization during heating for better interpretation of T_2 time constants, structural properties of 1 h-heated starch samples at varying temperatures were analyzed. For raw starches, the CLD profiles of debranched AP characterized by HPAEC-PAD (Fig. S1 and Table S1) showed that HAMS exhibited the highest average chain length of whole AP and the relative content of longer chains (fb2 and fb3, DP > 24), followed by WMS, and NMS.

The multi-scale structural data in Table 1 showed that, all starches underwent mainly starch hydration and swelling when heated at 40 °C, companied by decreased double helices. When temperature increased to 60 °C, WMS and NMS were partially gelatinized, with increased swelling power and water solubility, and reduced double helical content,

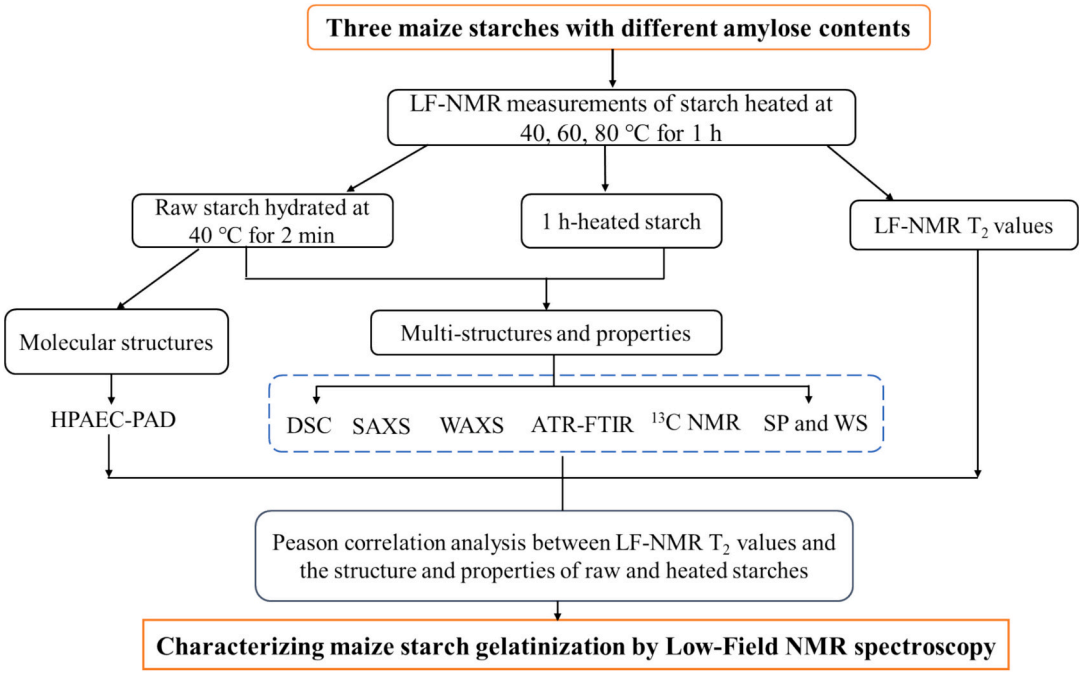

Fig. 1. Flow diagram of the experimental design of this study.

Table 1
Multi-scale structures of raw and 1 h-heated WMS, NMS, and HAMS [1].

Samples	T_o [2] (°C)	T_p [2] (°C)	T_c [2] (°C)	ΔH [2] (J/g)	Swelling power (g/g)	Water solubility (%)
WMS	64.8 ± 0.2^{e}	71.8 ± 0.1^{d}	77.4 ± 0.3^{c}	11.2 ± 0.6^{ab}	2.0 ± 0.0^{c}	1.4 ± 0.1^{def}
WMS-40	63.3 ± 0.5^{d}	70.8 ± 0.1^{e}	77.0 ± 0.1^{c}	11.6 ± 0.5^{a}	2.2 ± 0.0^{c}	2.0 ± 0.7^{cde}
WMS-60	66.3 ± 0.0^{c}	71.6 ± 0.1^{d}	77.1 ± 0.0^{c}	10.3 ± 0.4^{bc}	3.0 ± 0.1^{b}	2.7 ± 0.5^{c}
WMS-80	n. d.[3]	n. d.	n. d.	n. d.	5.9 ± 0.3^{a}	53.8 ± 1.0^{a}
NMS	64.8 ± 0.0^{e}	69.6 ± 0.1^{f}	73.9 ± 0.2^{d}	11.1 ± 0.1^{ab}	1.5 ± 0.0^{d}	0.7 ± 0.3^{f}
NMS-40	63.7 ± 0.4^{d}	68.3 ± 0.1^{g}	72.9 ± 0.0^{e}	10.4 ± 0.3^{b}	1.5 ± 0.1^{d}	1.3 ± 0.4^{def}
NMS-60	67.1 ± 0.3^{c}	69.6 ± 0.1^{f}	73.2 ± 0.1^{e}	9.3 ± 0.6^{c}	1.5 ± 0.1^{d}	2.2 ± 0.3^{cd}
NMS-80	n. d.	n. d.	n. d.	n. d.	5.7 ± 0.2^{a}	13.9 ± 0.3^{b}
HAMS	82.4 ± 0.2^{ab}	97.5 ± 0.1^{a}	110.7 ± 0.5^{a}	3.8 ± 0.4^{de}	1.3 ± 0.2 ^{d}	0.9 ± 0.0^{ef}
HAMS-40	81.8 ± 0.0^{b}	94.8 ± 0.1^{c}	109.6 ± 0.0^{b}	3.2 ± 0.0^{e}	1.4 ± 0.2^{d}	1.2 ± 0.4^{def}
HAMS-60	82.8 ± 0.8^{a}	96.8 ± 0.1^{b}	109.3 ± 0.2^{b}	3.0 ± 0.0^{e}	1.3 ± 0.1^{d}	2.2 ± 0.5^{cd}
HAMS-80	82.1 ± 0.0^{ab}	97.6 ± 0.5^{a}	109.4 ± 0.2^{b}	4.6 ± 0.9^{d}	2.1 ± 0.3^{c}	2.7 ± 0.4^{c}

Samples	Double helical content (%)	Single helical content (%)	Amorphous region content (%)	Total relative crystallinity (%)	FTIR ratio at 1047/1022 cm^{-1}
WMS	36.0	0.0	64.0	27.2 ± 0.2^{b}	0.72 ± 0.00^{ab}
WMS-40	32.0	0.0	68.0	31.0 ± 0.7^{a}	0.75 ± 0.01^{a}
WMS-60	27.0	0.0	73.0	23.8 ± 0.9^{c}	0.67 ± 0.00^{bc}
WMS-80	n. d. [2]	n. d.	100.0	n. d.	0.52 ± 0.00^{e}
NMS	34.4	3.6	62.0	23.9 ± 0.6^{c}	0.67 ± 0.01^{bc}
NMS-40	28.3	2.7	69.0	24.1 ± 0.4^{c}	0.66 ± 0.03^{abc}
NMS-60	25.6	2.4	72.0	20.8 ± 0.2^{d}	0.64 ± 0.05^{cd}
NMS-80	n. d.	n. d.	100.0	n. d.	0.51 ± 0.01^{e}
HAMS	26.1	12.9	61.0	20.1 ± 0.2^{d}	0.75 ± 0.03^{a}
HAMS-40	17.8	9.7	72.5	12.0 ± 0.1^{f}	0.62 ± 0.01^{cd}
HAMS-60	17.6	8.4	74.0	12.0 ± 1.2^{f}	0.60 ± 0.02^{d}
HAMS-80	17.6	8.4	74.0	14.4 ± 0.5^{e}	0.67 ± 0.03^{bc}

[1] Values are means ± SD. Values with different letters in the same column are significantly different at $p < 0.05$.
[2] T_o, onset temperature; T_p, peak temperature; T_c, conclusion temperature; ΔH, enthalpy change.
[3] n.d. = not detectable.

crystallinity and 1047/1022 ratio, while HAMS swelled with unchanged ordered structures compared to 40 °C. At 80 °C, WMS and NMS had fully gelatinization with the highest levels of swelling and starch solubilization, showing loss of double helices, crystalline and lamellar structures (Fig. S2), and disrupted granular structures (Fig. S3). While, HAMS presented a reorganized and more ordered structure (Table 1) at 80 °C with its granular structure remaining intact (Fig.S3).

3.2. Dynamic changes of proton mobility in starches heated at different temperatures

To understand dynamic changes in proton mobility during heating, the T_2 time constants of starch samples, were measured every two minutes by LF-NMR when heating at different temperatures (40, 60, and 80 °C) in excess water for 1 h. Exponential fitting (Fig. 2–4) of relaxation curves (Fig. S4) revealed three proton populations with varied relaxation times: 20–120 ms (T_{21}), 200–1400 ms (T_{22}), and 500–6000 ms (T_{23}). In a starch-water system, distinct proton populations arise from the varying microenvironments where protons are located, showing different mobilities. For example, protons inside starch granules exhibit slower mobility and consequently lower relaxation times compared to those outside the granules (Bosmans et al., 2012). The first proton population, T_{21} with the lowest relaxation time, represents the least mobile water protons, while the T_{22} and T_{23} correspond to the second and the most mobile water protons, respectively. Based on the distinct environments and previous reports, the T_{21} is assigned to confined water protons interacting with starch molecules in the intra-granular space (intra-granular water), where mobility is severely restricted by the dense polymer matrix (Bosmans et al., 2012; Kovrlija et al., 2020). T_{22} corresponds to the extra-granular water interacting with the starch chains located at the surface of the starch granule through hydrogen bonding or other weak interactions (extra-granular water on the granular surface). The most mobile T_{23} with 500–6000 ms (including the relaxation time of free water, 2–3 s at 40 °C (Bosmans et al., 2012)), is indicative of water present in a highly mobile environment. This fraction corresponds to free water or water interacting with leached starch molecules (i.e., free water or leached-starch interacting water).

3.2.1. T_2 time constants of raw starches during hydration in excess water

At initial heating stage (2 mins), the T_2 values of starches were similar across all temperatures as shown in Fig. 2–4, indicating that the starches only hydrated and possibly did not undergo significant structural changes in such a short duration, even at 80 °C. These data were therefore collected and shown in Table 2 to represent the water mobility and distributions in raw starches when incubated in excess water. The T_{21} and T_{22} values of WMS were the highest, followed by the NMS, while those of HAMS were the lowest, implying that AM molecules inhibited the water mobility of these two populations for raw starches hydrated in excess water. However, the T_{23} value of NMS was the highest, followed by WMS, while that of HAMS was the lowest, indicating no clear pattern for this population with increasing AC. This result also suggested that AC might be not the key factor affecting the mobility of the free water or leached-starch interacting water during hydration. The relative concentration of second proton population (M_{22}) for all starches were the highest among the three proton groups, followed by M_{21} and M_{23}, indicating that the extra-granular water protons at the granular surface were the dominant group during hydration, consistent with a previous report (Kovrlija et al., 2020). This is reasonable, as starch molecules located at the granule surface are the first to come into contact with water and subsequently interact with water protons during hydration. In addition, this starch-water interaction during hydration is driven mainly by flexible side chains on the starch granule surface (Baldwin et al., 2015). M_{22} values showed an increased trend with increasing AC, suggesting that increasing AC elevated the amount of this extra-granular water. This is attributed to the disordering effect of AM molecules on the granular structure (Zhong et al., 2022), damaging the ordered alignment of AP side chains, thereby resulting in more free chains exposed on the surface available to interact with water protons. However, the M_{21} and M_{23} values presented opposite trends to M_{22}, e.g. decreased with increasing AC (Table 2), reflecting the inhibition effects of AM on water absorption (Ding, Blennow, & Zhong, 2024). These data demonstrated that T_2 signals during hydration were largely affected by

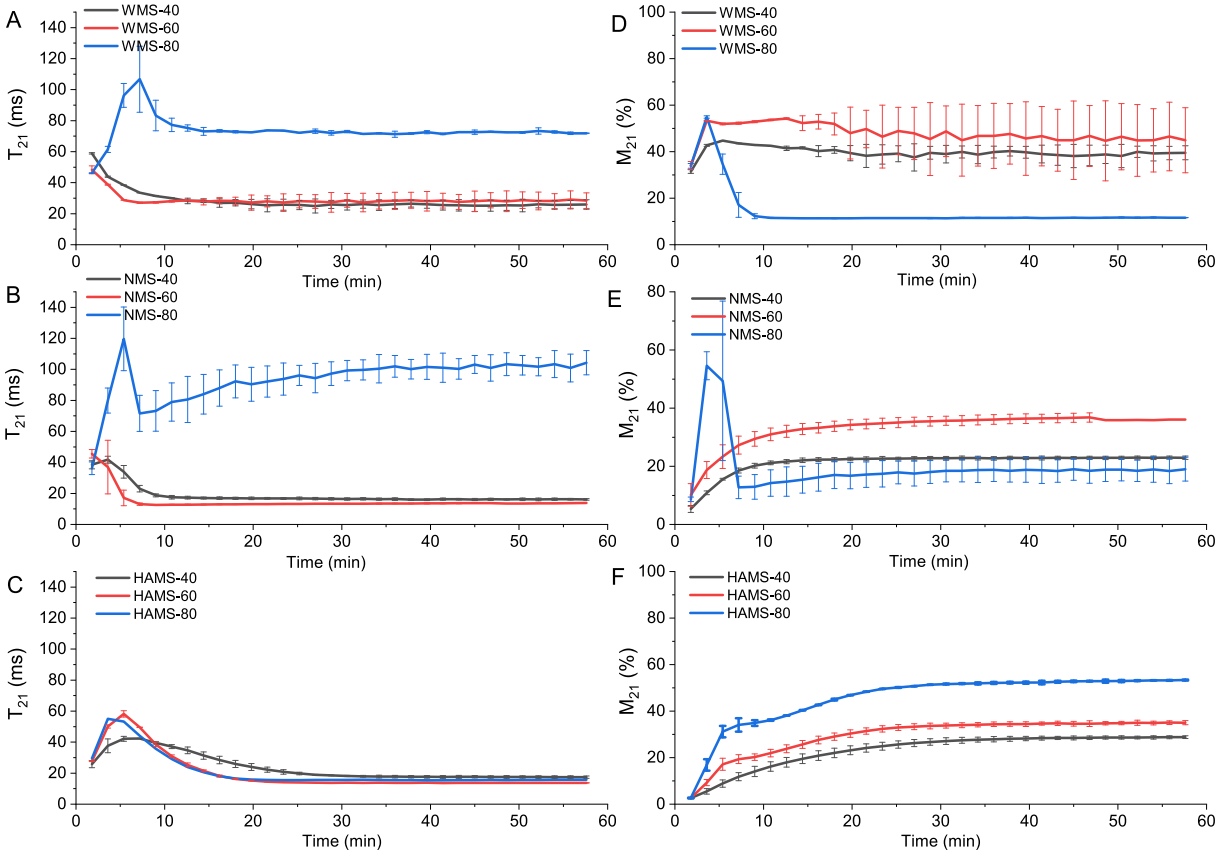

Fig. 2. T_{21} (A-C) and M_{21} (D-F) dynamics of starches during 1 h of heating at different temperatures in excess water.

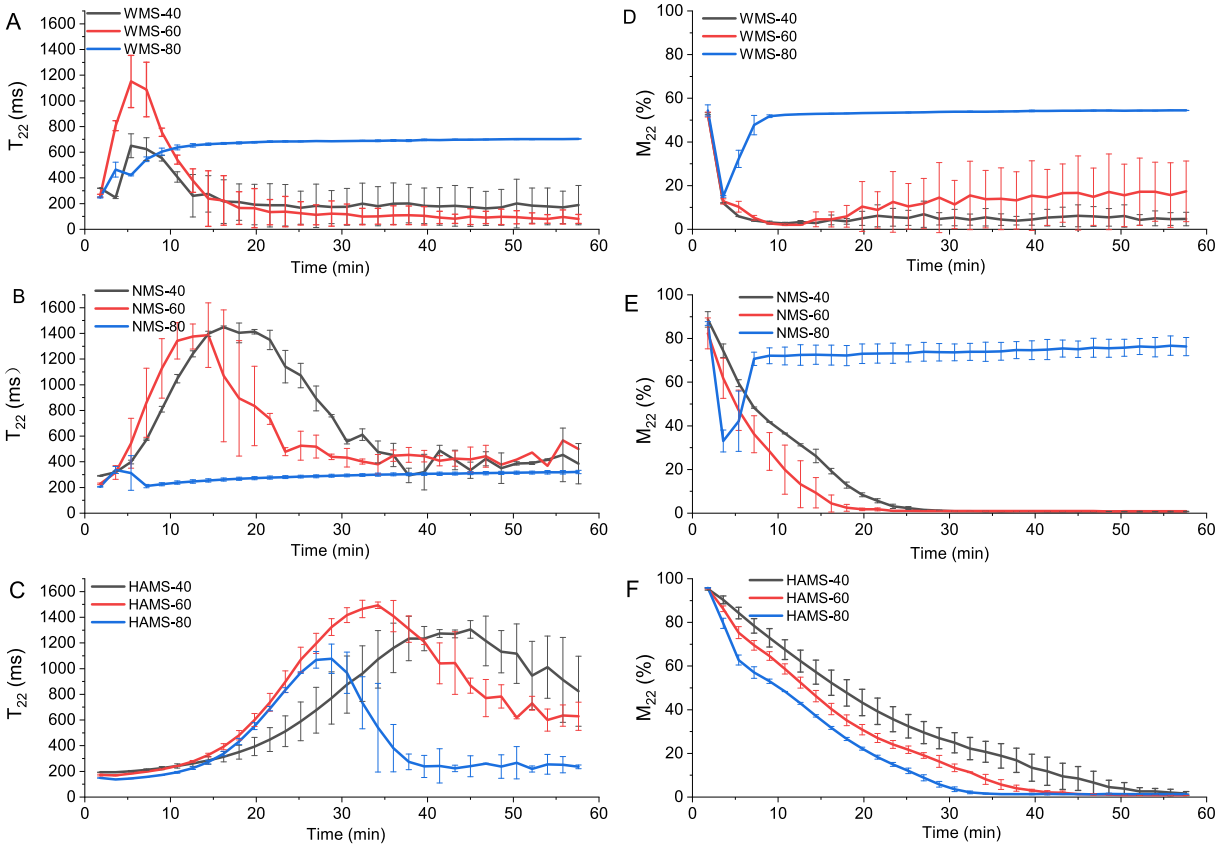

Fig. 3. T_{22} (A-C) and M_{22} (D-F) dynamics of starches during 1 h of heating at different temperatures in excess water.

the AC.

3.2.2. *Proton mobility dynamic in starches during 1 h of heating at different temperatures*

3.2.2.1. The least mobile water protons (T_{21} - intra-granular water). The dynamic changes in T_{21} time constants of starch samples during 1 h of heating in Fig. 2 mainly suggested at 40 °C and 60 °C, the T_{21} values for WMS and NMS (Fig. 2 A and B) decreased and then remained stable within the first 10 mins, although a slight increase in the T_{21} was observed for NMS-40 sample, while M_{21} increased and then plateaued within first 5 mins for WMS and first 10 mins for NMS (Fig. 2 D and E). At these two temperatures, WMS and NMS mainly swelled (section 3.1), and thus these results implied that starch swelling mainly happened in the first 10 mins of heating, leading to decreased mobility (lower T_{21}) but increased amount (higher M_{21}) of the intra-granular water protons. The decreased mobility indicated tightened interactions between starch and water molecules (Kovrlija et al., 2020). The increased M_{21} was attributed to water absorption and starch swelling. In addition, the decreased double helical content as shown in Table 1 indicated that the water reached the crystalline region, and disrupted the hydrogen bonds of the double helices after heating at 40 °C and 60 °C. At 80 °C, both T_{21} and M_{21} of WMS and NMS increased and then decreased to a stable value within the first 10 mins. The initial increase in T_{21} values was attributed to the thermal activation mechanism based on the Arrhenius' law (Kim & Cornillon, 2001). While, the subsequent decrease was due to dramatically increased viscosity in the starch paste caused by the fully swelling and complete gelatinization (Table 1). Similarly, as discussed above, the initial increases in the M_{21} values of WMS and NMS at 80 °C were related to water absorption and granular swelling, and the further decrease in M_{21} was attributed to fully starch gelatinization (Nivelle, Beghin, et al., 2019). Full gelatinization resulted in crystals melting (Table 1, no crystallinity) and granule disruption, thus, fewer intact starch granules (Fig. S3, mainly broken and disrupted granules) were available to interact with water molecules at the intra-granular space.

However, T_2 signals of HAMS behaved differently from those of WMS and NMS but similar across all temperatures, indicating its unique and thermally stable structures within 40–80 °C, attributed to its higher AC. Specifically, T_{21} values of HAMS (Fig. 2 C) increased and then decreased to a stable value within 30 mins, whereas the M_{21} of HAMS (Fig. 2 F) significantly increased within 20 mins and then remained stable during the last 40 mins. The initial increase in T_{21} at all three temperatures for HAMS was attributed to the thermal activation mechanism, and the subsequent decrease was attributed to the tightened interaction between the water and starch molecules during the swelling, limiting the proton movement. Notably, no initial increase in the T_{21} values of NMS-60, WMS-40 and WMS-60 samples suggested that the thermal activation at lower temperatures was overruled by other factors, such as strengthened interactions between water protons and starch in the intra-granular space resulted from the starch swelling, supported by the swelling power data in Table 1. In addition, the increased M_{21} and no further decrease at all temperatures indicated swelling and no gelatinization, supported by their structural changes in section 3.1. No change in the helical content but decreased single helical content of HAMS at all temperatures further suggested that for this high AM type of starch, water mainly is absorbed into the amorphous regions and disrupts the single helices but does not alter the crystalline region. Hence, at temperatures below gelatinization, such as 40 °C and 60 °C, granular swelling of WMS and NMS primarily occurred within the first 10 min of heating, characterized by an increase in the amount of intra-granular water protons and a corresponding decrease in their mobility. At temperatures above gelatinization, such as 80 °C, these two starches underwent both swelling and gelatinization within the first 10 min of heating. During the swelling stage, higher amounts of intra-granular

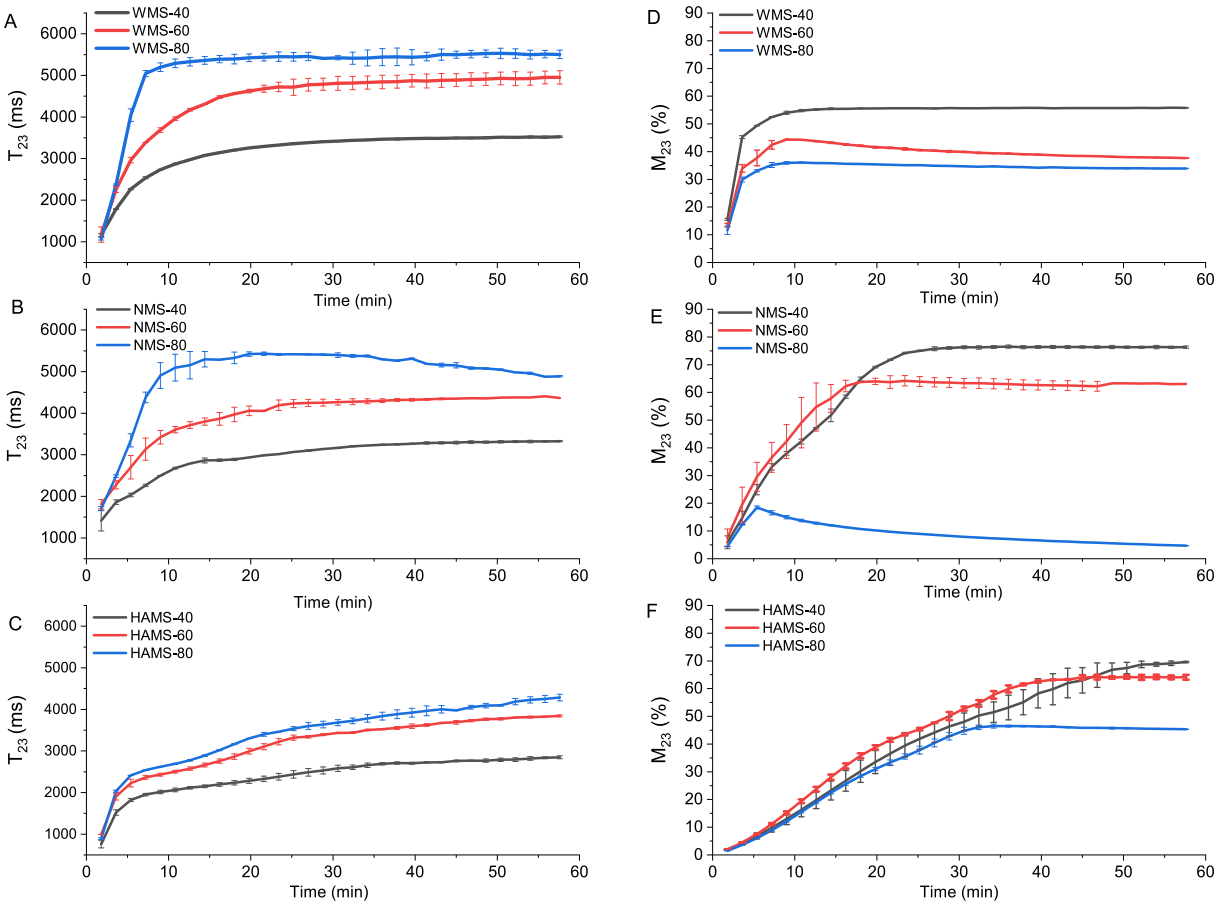

Fig. 4. T_{23} (A-C) and M_{23} (D-F) dynamics of starches (10 % *w*/w) during 1 h of heating at different temperatures in excess water.

Table 2
T_2 LF-NMR parameters for raw starches hydrated at 40 °C for 2 mins [1].

Starches	T_{21} (ms)	T_{22} (ms)	T_{23} (ms)	M_{21} (%)	M_{22} (%)	M_{23} (%)
WMS	58.9 ± 0.4^{a}	320.2 ± 1.7^{a}	1164.3 ± 34.3^{ab}	31.5 ± 0.8^{a}	53.0 ± 0.5^{b}	15.6 ± 0.3^{a}
NMS	38.5 ± 2.6^{b}	291.4 ± 3.4^{b}	1418.5 ± 248.6^{a}	5.3 ± 1.2^{b}	88.8 ± 3.5^{a}	5.9 ± 2.3^{b}
HAMS	25.8 ± 2.3^{c}	193.3 ± 0.1^{c}	760.9 ± 93.0^{c}	2.6 ± 0.4^{b}	95.3 ± 0.5^{a}	2.1 ± 0.2^{b}

[1] Values are means ± SD. Values with different letters in the same column are significantly different at $p < 0.05$.

water protons with greater mobility were absorbed due to the disordering of the helical structure. During the later gelatinization stage, the amounts and mobility of intra-granular water protons decreased due to gelation. For HAMS, only the swelling stage occurred across all temperatures.

3.2.2.2. The second mobile water protons (T_{22} - extra-granular water on the granular surface). At 40 °C and 60 °C, the T_{22} values increased to maximum values within the first 5 mins for WMS and 15 mins for NMS, and 30 mins for HAMS, and then decreased until reaching a plateau (Fig. 3 A - C). The M_{22} values correspondingly decreased to around 10 % (Fig. 3 D - E), opposite to the increasing trend of M_{21}. These changes suggested that the granular swelling is promoted by the movement of water protons from the granular surface to the internal region of granules. It also indicated that higher AC inhibited such water movement, thereby slowing down the starch swelling (Nivelle, Remmerie, et al., 2019). Interestingly, at 80 °C, M_{22} values of WMS and NMS remarkably decreased and then increased within the first 10 mins, still opposite to the trend of M_{21} values. The first decrease was attributed to the starch swelling, leading to more water moved from the granular surface into intra-granular space. While, at the later stage of gelatinization, the granular disruption of NMS and WMS led to many fragments with larger surface (Fig. S3), which can serve as core to interact with water protons in the fragment surface by forming gelation network structure, thereby inducing increased M_{22}. However, at 80 °C, the tendency of T_{22} and M_{22} in HAMS was similar to that at 40 °C and 60 °C, but the T_{22} peak appeared earlier, due to the effects of high temperature on promoting starch swelling (Zhang et al., 2021). Therefore, at 40 °C and 60 °C, water protons on the granular surface migrated to the internal granule regions during the swelling process, a process that was retarded and prolonged by higher AC. At 80 °C, a similar migration occurred during the initial swelling stage. However, after gelatinization, these water protons migrated back to the granular surface in WMS and NMS. In contrast, HAMS exhibited only the swelling stage, with no evidence of gelatinization due to its high thermal stability.

3.2.2.3. The most mobile water protons (T_{23} - free water or leached starch interacting water). The dynamic change trends of T_{23} were similar across all starches, e.g., T_{23} increased during the first 30 mins at all temperatures (Fig. 4 A - C), showing higher mobility of the free water or leached starch interacting water (Nivelle, Remmerie, et al., 2019; Rondeau-Mouro et al., 2014). Additionally, T_{23} increased with increasing heating

temperatures, aligning with Arrhenius' law, suggesting that elevated temperatures enhanced the mobility of this type of water protons (Nivelle, Beghin, et al., 2019). M_{23} significantly increased and reached a plateau at all temperatures as the incubation time increased. With increasing incubation time, starch swelling and gelatinization were enhanced, resulting in more intra-granular water (as indicated by increased M_{21} at 40 and 60 °C) and more extra-granular water at the surface (as indicated by increased M_{22} at 80 °C). This process is expected to decrease the amount of free water. Therefore, the observed results can be attributed to the fact that prolonged incubation promotes starch leaching (as supported by the water solubility data in Table 1), thereby increasing the amount of water protons interacting with these leached starch molecules. Interestingly, the peak values for M_{23} decreased with increasing temperatures (Fig. 4 D - F), opposite to the increasing trend observed for the water solubility (Table 1). This further suggests that, in addition to leached starch, free water also constitutes a portion of the water protons associated with the T_{23} component. Again, higher temperature induced greater swelling and starch gelatinization, more water was occupied to interacted with starch molecules at both intra-granular space and granular surface, thereby leading to less free water or water interacting with leached starches.

3.2.3. T_2 time constants of 1 h-heated starches

To clearly visualize the changes in T_2 relaxation behaviors of final products, T_2 distributions of three starches at the end of 1 h-heating were extracted and plotted in Fig. 5. These results mainly indicated that at 40 and 60 °C, T_{21} of NMS and HAMS were lower than that of WMS, and T_{22} increased while T_{23} decreased with increasing AC, suggesting decreased mobility of intra-granular water protons (T_{21}) and free water or leached starch interacted water protons (T_{23}), but increased mobility of extra-granular water protons (T_{22}) with higher AC. AM molecules function on restricting the movement of intra-granular water protons, and free water or water interacting with leached starches, due to the ability of AM to inhibit swelling and form a network structure after leaching, thereby limiting water proton movement. In contrast, the increased mobility of extra-granular water on granular surface with higher AC can be attributed to the greater number of flexible side chains on the granule surface (Baldwin et al., 2015), resulting from the disordering effect of AM. Relative proton concentrations of NMS and HAMS were similar, with M_{21} and M_{22} being lower while M_{23} higher than WMS. Thus, higher AC lowered the amounts of water protons both interacted with internal and surface regions of starch granules, while induced higher amount of free water or water protons interacting with leached starches at 40 and 60 °C. At these two temperatures, water hydration, granular swelling, and partial gelatinization were the major phenomenon (Table 1), which are inhibited by AM molecules (Nivelle, Remmerie, et al., 2019; Zhong, Qu, et al., 2022; Zhu et al., 2016). The above results suggested that the well-known inhibition effect of AM on the starch swelling is attributed to the decreased water interacted with starches in the intra-granular and extra-granular surface space. At 80 °C, HAMS had lower water mobility of all three types of water protons and lower contents of extra-granular water on granular surface but higher contents of intra-granular, and free water or leached starch interacting water protons, compared to NMS and WMS. In gelatinized starch system, AM acts structural element that reduces the mobility (Nivelle, Remmerie, et al., 2019). In addition, HAMS with higher AC kept granular integrity (Fig.S3), whereas WMS and NMS lost their granular structure at 80 °C. These findings indicated that the T_2 relaxation behaviors of starch during heating were also affected by the AC to some extent, supporting our hypothesis.

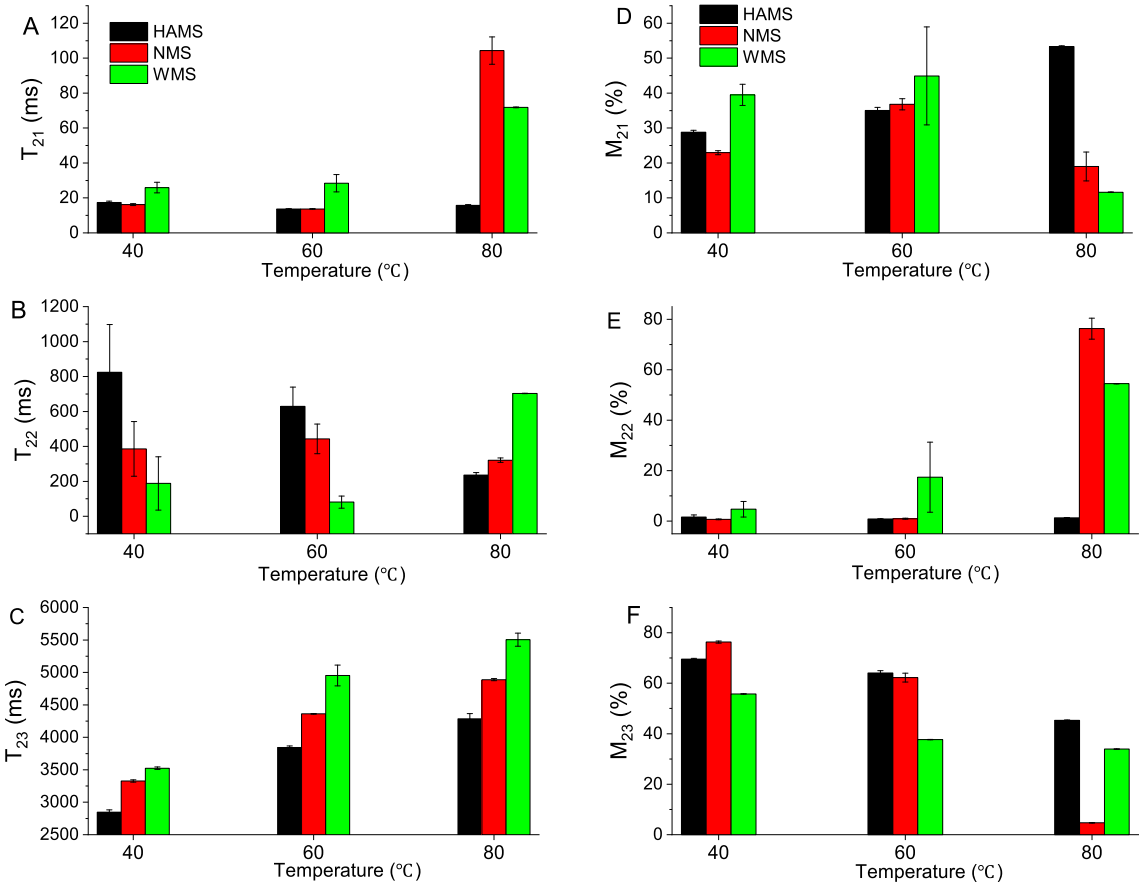

Fig. 5. T_2 values of 1 h-heated starches at different temperatures.

3.3. Pearson correlation analysis between T_2 values and structures and properties of starches

3.3.1. Raw starches

To give intuitive relationships between the T_2 time constants (Table 1) and starch parameters only heated at 40 °C for 2 mins (which represent raw starches), Pearson correlation was conducted between them, as shown in Fig. 6 A. As expected, AC weakly and negatively correlated with all T_2 values, except for the M_{22} with weak positive correlation. This is attributed to that AM inhibited the water movement, and slowed down starch hydration and swelling. Compared to AC, T_2 values had more significant correlations with chain-length distribution, helical and lamellar structural parameters.

T_{21} was significantly and positively correlated with the relative content of amorphous region (AR), indicated that amorphous region promoted the mobility of intra-granular water during hydration. This is attributed to that amorphous region is flexible while the crystalline region is rigid and compact due to the dense packing of double helices (Donmez, Pinho, Patel, Desam, & Campanella, 2021; Tang, Godward, & Hills, 2000). M_{21} was positively correlated with the thickness of amorphous lamellae (da) and AR, suggesting that amorphous lamellae were the dominant place interacting with water protons during hydration, and more and thicker amorphous region can accommodate higher content of intra-granular water, consistent with a previous report (Jia et al., 2023). T_{22} had a significantly positive correlation with double helical content (DH) but a negative correlation with single helical content (SH), indicating that more double helices but fewer single helices contributed to higher mobility of water on the granular surface. Double helices pack and align in the crystalline region as ordered structure, while single helices are crystalline defects in the crystalline region (Ding et al., 2023; Zhong et al., 2021). More double and less single helices indicated a more ordered structure with less AM molecules (Jia et al., 2023), which reasonably promoting the mobility of water protons on the granular surface. Surprisingly, T_{23} was positively correlated with relative content (RC) of fb1 (RC_{fb1}, DP 13–24) and fa (RC_{fa}, DP 6–12), but negatively related to average chain length (ACL) of fa (ACL_{fa}). This suggested that AP molecules mainly leached out during the hydration; especially, those short fa and fb1 chains were the main chains leached and then interacted with water protons (Ding et al., 2024). This result also explained the no clear pattern in T_{23} with increasing AC as discussed in section 3.2.1. In addition, the positive correlation between M_{23} and AR further implied that the molecules in the amorphous region possibly were the main molecules leaching out during the hydration.

3.3.2. 1 h-heated starches

To clarify the relationships between T_2 time constants (section 3.2.3) and starch structural parameters (section 3.1) associated with swelling and gelatinization, Pearson correlations were conducted on starch samples heated for 1 h. Results in Fig. 6 B showed T_2 signals were significantly correlated multiple gelatinization properties, supporting our hypothesis. T_{21} and T_{23} had similar correlations, although some correlations of T_{23} were less significant due to that free water is also part of water protons in T_{23}. They were negatively correlated with total relative crystallinity (TRC), double helix content (DH), the FTIR 1047/1022 absorbance ratio, and all SAXS parameters (D, d_c, d_a and d_{ac}), as well as gelatinization temperatures (T_o, T_p and T_c). These correlations indicated that ordered structures with thicker lamella and higher thermal stability inhibited the mobility of intra-granular and free water or leached-starch interacting water protons. Compact crystalline structures with strong inter-chain bonds restrict water-starch interactions, slowing swelling, gelatinization, and granule disruption during heating (Liu, Hao, Chen, & Gao, 2019; Zhang et al., 2021). Thus, such starches were related to reduced water movement within intra-granular spaces and at the granule surface during heating. Conversely, they positively correlated with AR and SP, indicating that more amorphous region and higher degree of swelling promoted their mobility. M_{21} and M_{23} also demonstrated similar correlation patterns, opposite to those of M_{22}. Both M_{21} and M_{23} showed positive correlations with all SAXS parameters, the 1047/1022 ratio, and gelatinization temperatures, and negative correlations with AR. These results further suggested that ordered crystalline regions absorbed water protons during heating, with higher thermal stability and thicker lamella allowing these areas to retain more water protons. Additionally, starches with such ordered structures also had more free water or water interacting with leached starches. During swelling and gelatinization, water protons redistributed between the intra-granular and extra-granular water, thereby showing opposite correlations of M_{22} compared to M_{21}.

4. Conclusion

Proton mobility of maize starches with different ACs during heating at different temperatures (40–80 °C) were monitored by LF-NMR to build relations between the T_2 time constants and gelatinization properties. Three groups of water protons with distinct relaxation times were identified to interact with starches: 20–120 ms (T_{21}), 200–1400 ms (T_{22}), and 500–6000 ms (T_{23}), representing the intra-granular water, extra-granular water on the granular surface, and free water or leached-starch interacting water, respectively. In raw starches hydrated in excess water, T_{22} signals dominated, and increasing AC reduced all three T_2 values, demonstrating effect of AM molecules on limiting water mobility. When heating in excess water, at swelling stage, M_{22} values significantly decreased, while M_{21} values increased, indicating that granular swelling is facilitated by the movement of water protons from the surface into the granule interior. At the following gelatinization stage, M_{21} further decreased while M_{22} increased, suggesting that water protons moved back to granular surface due to the disrupted granular structure. Pearson correlations analysis further showed that M_{21} was positively correlated with relative content of amorphous region in raw starches, while after heating, M_{21} had positive correlations with FTIR 1047/1022 ratio of the absorbances and gelatinization temperatures, suggesting that the amorphous region absorbed water during hydration, while ordered crystalline region serves as the storage site for water protons during heating. This study demonstrates significant changes in the mobility and distribution of starch-relevant water protons during heating, as observed via LF-NMR, enhancing our understanding of the swelling and gelatinization of maize starches. For example, it highlighted that AM molecules restrict granular swelling by reducing the amount of water protons interacting with both the internal and surface regions of starch granules during heating, although the underlying mechanism requires future investigation. This study is expected to facilitate the application of LF-NMR in understanding starch properties, such as gelation and retrogradation, from the perspective of starch molecule-water interactions in the future. However, the LF-NMR temperature limitation of only 90 °C may restrict its applicability for studying high-AM starches, which typically require higher temperatures for complete gelatinization.

CRediT authorship contribution statement

Li Ding: Writing – review & editing, Writing – original draft, Validation, Software, Methodology, Investigation, Conceptualization. **Samira Ebrahimi:** Writing – review & editing, Methodology, Investigation. **Xingxun Liu:** Writing – review & editing. **Staffan Persson:** Writing – review & editing. **Jacob Judas Kain Kirkensgaard:** Writing – review & editing, Methodology. **Kasper Enemark-Rasmusse:** Writing – review & editing, Methodology. **Jinhui Chang:** Writing – review & editing. **Sheng Chen:** Writing – review & editing. **Andreas Blennow:** Writing – review & editing, Resources. **Tomasz Pawel Czaja:** Writing – review & editing, Methodology, Investigation, Conceptualization. **Yuyue Zhong:** Writing – review & editing, Writing – original draft, Supervision, Resources, Project administration, Conceptualization.

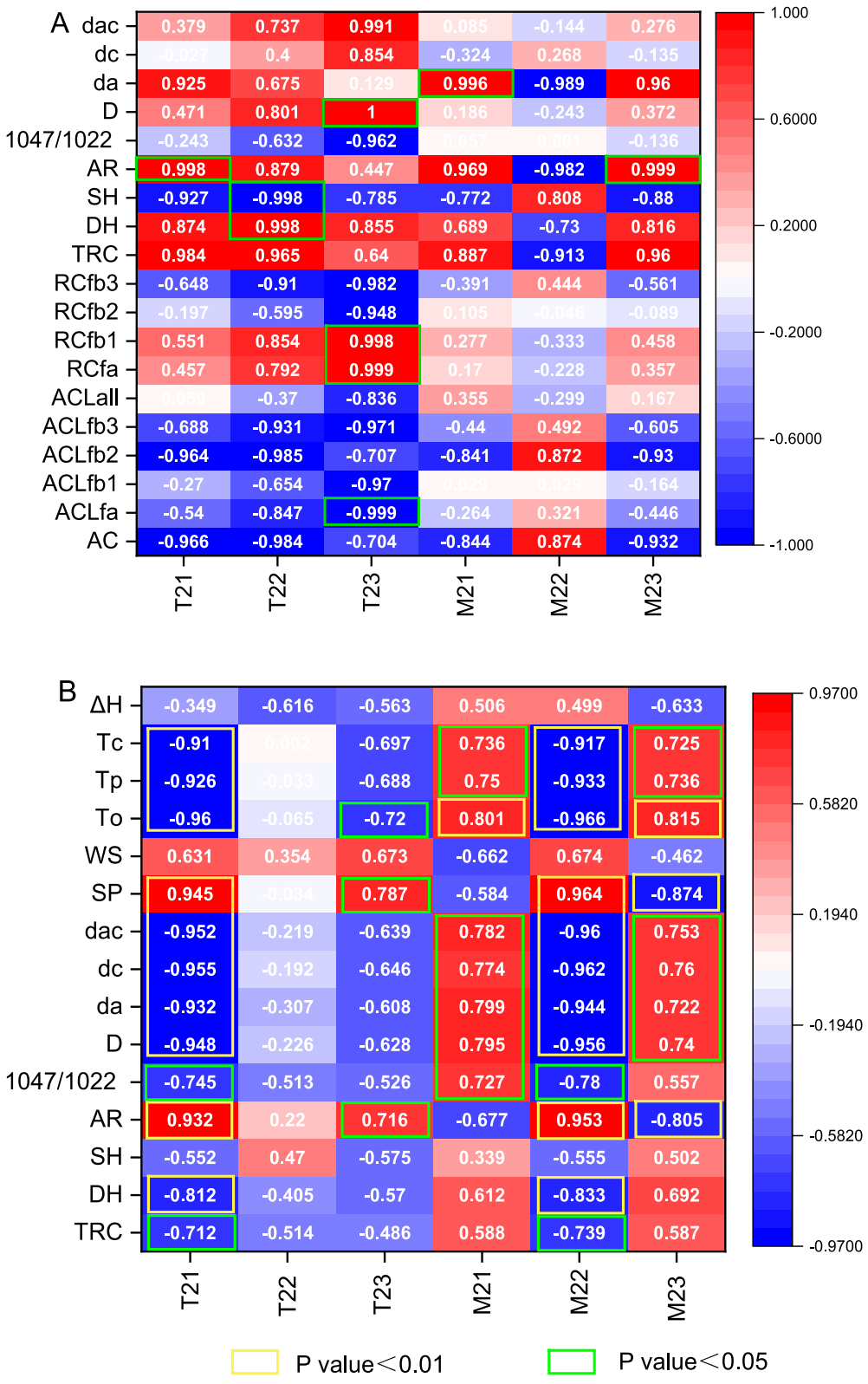

Fig. 6. Pearson correlation analysis between the LF-NMR T_2 values and structural parameters of raw (A) and 1 h-heated (B) starch samples (AC, amylose content; ACL_X, average chain lengths (DP) of fraction X; RC_X, relative amount of fraction X; *fa*, amylopectin chains with DP 6–12; fb_1, amylopectin chains with DP 13–24; fb_2, amylopectin chains with DP 25–36; fb_3, amylopectin chains with DP > 36; TRC, total relative crystallinity; SH, relative amount of single helices; DH, relative amount of double helices; AR, relative content of amorphous region; D, Bragg lamellar repeat distance; d_a, thickness of amorphous lamellae; d_c, thickness of crystalline lamellae; d_{ac}, long period distance; SP: swelling power; WS: water solubility. T_o, onset temperature; T_p, peak temperature; T_c, conclusion temperature; ΔH, enthalpy change.)

Declaration of competing interest

The authors declare that they have no known competing financial interests or personal relationships that could have appeared to influence the work reported in this paper.

Acknowledgements

Li Ding would like to thank the China Scholarship Council funding (CSC, 202006150028) for her PhD study at the University of Copenhagen, Denmark. The imaging data were collected at the Center for Advanced Bioimaging (CAB) Denmark. The WAXS and SAXS Data were generated was generated via a research infrastructure at the University of Copenhagen, partly funded by FOODHAY (Food and Health Open Innovation Laboratory, Danish Roadmap for Research Infrastructure). Staffan Persson acknowledges Villum Investigator (grant no. 25915), DNRF Chair (grant no. DNRF155), Novo Nordisk Laureate (grant no. NNF19OC0056076), Novo Nordisk Emerging Investigator (grant no. NNF20OC0060564), and Novo Nordisk Data Science (grant no. NNF0068884) grants.

Appendix A. Supplementary data

Supplementary data to this article can be found online at https://doi.org/10.1016/j.carbpol.2025.124292.

Data availability

Data will be made available on request.

References

Ai, Y., & Jane, J.-l. (2015). Gelatinization and rheological properties of starch. *Starch - Stärke, 67*(3–4), 213–224.

Baldwin, A. J., Egan, D. L., Warren, F. J., Barker, P. D., Dobson, C. M., Butterworth, P. J., & Ellis, P. R. (2015). Investigating the mechanisms of amylolysis of starch granules by solution-state NMR. *Biomacromolecules, 16*(5), 1614–1621.

Bosmans, G. M., Lagrain, B., Deleu, L. J., Fierens, E., Hills, B. P., & Delcour, J. A. (2012). Assignments of proton populations in dough and bread using NMR relaxometry of starch, gluten, and flour model systems. *Journal of Agricultural and Food Chemistry, 60*(21), 5461–5470.

Ding, L., Blennow, A., & Zhong, Y. (2024). Differential roles of C-3 and C-6 phosphate monoesters in affecting potato starch properties. *Grain & Oil Science and Technology, 7*, 79–86.

Ding, L., Huang, Q., Li, H., Wang, Z., Fu, X., & Zhang, B. (2019). Controlled gelatinization of potato parenchyma cells under excess water condition: structural and in vitro digestion properties of starch. *Food & Function, 10*(9), 5312–5322.

Ding, L., Liang, W., Qu, J., Persson, S., Liu, X., Herburger, K., & Zhong, Y. (2023). Effects of natural starch-phosphate monoester content on the multi-scale structures of potato starches. *Carbohydrate Polymers, 310*, Article 120740.

Donmez, D., Pinho, L., Patel, B., Desam, P., & Campanella, O. H. (2021). Characterization of starch–water interactions and their effects on two key functional properties: starch gelatinization and retrogradation. *Current Opinion in Food Science, 39*, 103–109.

Doona, C. J., & Baik, M.-Y. (2007). Molecular mobility in model dough systems studied by time-domain nuclear magnetic resonance spectroscopy. *Journal of Cereal Science, 45*(3), 257–262.

Guo, K., Tian, Y., Podzimska-Sroka, D., Kirkensgaard, J. J. K., Herburger, K., Enemark-Rasmussen, K., & Zhong, Y. (2024). Structural evolution of maize starches with different amylose content during pasting and gelation as evidenced by Rapid Visco Analyser. *Food Chemistry, 461*, Article 140817.

Jia, R., Cui, C., Gao, L., Qin, Y., Ji, N., Dai, L., & Sun, Q. (2023). A review of starch swelling behavior: Its mechanism, determination methods, influencing factors, and influence on food quality. *Carbohydrate Polymers, 321*, Article 121260.

Kim, Y.-R., & Cornillon, P. (2001). Effects of temperature and mixing time on molecular mobility in wheat dough. *LWT - Food Science and Technology, 34*(7), 417–423.

Kirtil, E., Cikrikci, S., McCarthy, M. J., & Oztop, M. H. (2017). Recent advances in time domain NMR & MRI sensors and their food applications. *Current Opinion in Food Science, 17*, 9–15.

Kovrlija, R., Goubin, E., & Rondeau-Mouro, C. (2020). TD-NMR studies of starches from different botanical origins: Hydrothermal and storage effects. *Food Chemistry, 308*, Article 125675.

Kuang, Q., Xu, J., Liang, Y., Xie, F., Tian, F., Zhou, S., & Liu, X. (2017). Lamellar structure change of waxy corn starch during gelatinization by time-resolved synchrotron SAXS. *Food Hydrocolloids, 62*, 43–48.

Li, C. (2022). Recent progress in understanding starch gelatinization - An important property determining food quality. *Carbohydrate Polymers, 293*, Article 119735.

Liu, K., Hao, Y., Chen, Y., & Gao, Q. (2019). Effects of dry heat treatment on the structure and physicochemical properties of waxy potato starch. *International Journal of Biological Macromolecules, 132*, 1044–1050.

Luallen, T. (2018). Chapter 13 - Utilizing Starches in Product Development. Eds.. In M. Sjöö, & L. Nilsson (Eds.), *Starch in Food* (2nd ed., pp. 545–579). Woodhead Publishing

Nivelle, M. A., Beghin, A. S., Bosmans, G. M., & Delcour, J. A. (2019). Molecular dynamics of starch and water during bread making monitored with temperature-controlled time domain 1H NMR. *Food Research International, 119*, 675–682.

Nivelle, M. A., Remmerie, E., Bosmans, G. M., Vrinten, P., Nakamura, T., & Delcour, J. A. (2019). Amylose and amylopectin functionality during baking and cooling of bread prepared from flour of wheat containing unusual starches: A temperature-controlled time domain (1)H NMR study. *Food Chemistry, 295*, 110–119.

Rondeau-Mouro, C., Cambert, M., Kovrlija, R., Musse, M., Lucas, T., & Mariette, F. (2014). Temperature-associated proton dynamics in wheat starch-based model systems and wheat flour dough evaluated by NMR. *Food and Bioprocess Technology, 8*(4), 777–790.

Serial, M. R., Blanco Canalis, M. S., Carpinella, M., Valentinuzzi, M. C., Leon, A. E., Ribotta, P. D., & Acosta, R. H. (2016). Influence of the incorporation of fibers in biscuit dough on proton mobility characterized by time domain NMR. *Food Chemistry, 192*, 950–957.

Sikora, M., Kowalski, S., Krystyjan, M., Ziobro, R., Wrona, P., Curic, D., & LeBail, A. (2010). Starch gelatinization as measured by rheological properties of the dough. *Journal of Food Engineering, 96*(4), 505–509.

Tang, H. R., Godward, J., & Hills, B. (2000). The distribution of water in native starch granules—a multinuclear NMR study. *Carbohydrate Polymers, 43*(4), 375–387.

Thygesen, L. G., Blennow, A., & Engelsen, S. B. (2003). The effects of amylose and starch phosphate on starch gel retrogradation studied by Low-field ^{1}H NMR relaxometry. *Starch - Stärke, 55*(6), 241–249.

Tian, Y., Liu, X., Kirkensgaard, J. J. K., Khakimov, B., Enemark-Rasmussen, K., Hebelstrup, K. H., & Zhong, Y. (2024). Characterization of different high amylose starch granules. Part I: Multi-scale structures and relationships to thermal properties. *Food Hydrocolloids, 146*.

Vickovic, D., Czaja, T. P., Gaiani, C., Pedersen, S. J., Ahrné, L., & Hougaard, A. B. (2023). The effect of feed formulation on surface composition of powders and wall deposition during spray drying of acidified dairy products. *Powder Technology, 418*.

Wang, S., & Copeland, L. (2013). Molecular disassembly of starch granules during gelatinization and its effect on starch digestibility: a review. *Food & Function, 4*(11), 1564–1580.

Wang, S., Zhang, X., Wang, S., & Copeland, L. (2016). Changes of multi-scale structure during mimicked DSC heating reveal the nature of starch gelatinization. *Scientific Reports, 6*, Article 28271.

Wu, Y., Fan, D., Gao, Y., Ma, S., Yan, B., Lian, H., & Zhang, H. (2018). Study on water proton distribution and flow status of starch during the hydration process. *International Journal of Biological Macromolecules, 118*(Pt A), 997–1003.

Xu, J., Li, Z., Zhong, Y., Zhou, Q., Lv, Q., Chen, L., … Liu, X. (2021). The effects of molecular fine structure on rice starch granule gelatinization dynamics as investigated by in situ small-angle X-ray scattering. *Food Hydrocolloids, 121*, Article 107014.

Zhang, B., Wang, K., Hasjim, J., Li, E., Flanagan, B. M., Gidley, M. J., & Dhital, S. (2014). Freeze-drying changes the structure and digestibility of B-polymorphic starches. *Journal of Agricultural and Food Chemistry, 62*(7), 1482–1491.

Zhang, B., Zhang, Q., Wu, H., Su, C., Ge, X., Shen, H., … Li, W. (2021). The influence of repeated versus continuous dry-heating on the performance of wheat starch with different amylose content. *LWT - Food Science and Technology, 136*, Article 110380.

Zhong, Y., Li, Z., Qu, J., Bertoft, E., Li, M., Zhu, F., & Liu, X. (2021). Relationship between molecular structure and lamellar and crystalline structure of rice starch. *Carbohydrate Polymers, 258*, Article 117616.

Zhong, Y., Qu, J., Li, Z., Tian, Y., Zhu, F., Blennow, A., & Liu, X. (2022). Rice starch multi-level structure and functional relationships. *Carbohydrate Polymers, 275*, Article 118777.

Zhong, Y., Tai, L., Blennow, A., Ding, L., Herburger, K., Qu, J., & Liu, X. (2022). High-amylose starch: Structure, functionality and applications. *Critical Reviews in Food Science and Nutrition*, 1–23.

Zhu, D., Zhang, H., Guo, B., Xu, K., Dai, Q., Wei, C., & Huo, Z. (2016). Effect of nitrogen management on the structure and physicochemical properties of rice starch. *Journal of Agricultural and Food Chemistry, 64*(42), 8019–8025.